Assessing national exposure and impact to glacial lake outburst floods considering uncertainty under data sparsity

Huili Chen[1], Qiuhua Liang[1], Jiaheng Zhao[2], Sudan Bikash Maharjan[3]

[1] School of Architecture, Building and Civil Engineering, Loughborough University, Loughborough LE11 3TU, UK

5 [2] FM Global, 117369, Singapore

[3] International Centre for Integrated Mountain Development (ICIMOD), Nepal

Correspondence to: Qiuhua Liang (Q.Liang@lboro.ac.uk)

Abstract. Glacial Lake Outburst Floods (GLOFs) are widely recognized as one of the most devastating natural hazards in the Himalayas, with catastrophic consequences including substantial loss of life. To effectively mitigate these risks and enhance
10 regional resilience, it is imperative to conduct an objective and holistic assessment of GLOF hazards and their potential impacts over a large spatial scale. However, this is challenged by the limited availability of data and the inaccessibility to most of the glacial lakes in high-altitude areas. The data challenge is exacerbated when dealing with multiple lakes across an expansive spatial area. This study aims to exploit remote sensing techniques, well-established Bayesian regression models for estimating glacial lake conditions, cutting-edge flood modeling technology, and open data from various sources to innovate a framework
15 for assessing the national exposure and impact of GLOFs. In the innovative framework, multi-temporal imagery is utilized with a Random Forest model to extract glacial lake water surfaces. Bayesian models, derived from previous research, are employed to estimate a plausible range of glacial lake water volumes and associated GLOF peak discharges while accounting for the uncertainty stemming from the limited size of available data and outliers within the data. A significant number of GLOF scenarios is subsequently generated based on this estimated plausible range of peak discharges. A graphics processing unit
20 (GPU)-based hydrodynamic model is then adopted to simulate the resulting flood hydrodynamics in different GLOF scenarios. Necessary socio-economic information is collected and processed from multiple sources, including OpenStreetMap, Google Earth, local archives, and global data products, to support exposure analysis. Established depth-damage curves are used to assess the GLOF damage extents to different exposures. The evaluation framework is applied to 21 glacial lakes identified as potentially dangerous in the Nepal Himalayas. The results indicate that Tsho Rolpa Lake, Thulagi Lake, and Lower Barun
25 Lake bear the most serious impacts of GLOFs on buildings and roads, and influence existing hydropower facilities, while Tsho Rolpa Lake, Lower Barun Lake, and Lumding Lake will experience the most impacts of GLOFs on agriculture areas. Five anonymous lakes (located at 85°37′51″ E, 28°09′44″ N; 87°44′59″ E, 27°48′57″ N; 87°56′05″ N, 27°47′26″ E; 86°55′41″ E, 27°51′00″ N; 86°51′29″ E, 27°41′13″ N) have the potential to impact more than 200 buildings, and the first three lakes may even submerge existing hydropower facilities.

30 # 1 Introduction

Glacial Lake Outburst Floods (GLOFs) are recognized as one of the most impactful natural hazards in the Himalayas, where these disasters have had the highest death toll worldwide and caused serious economic damage (Veh et al., 2020). GLOFs can generate transient discharges that are orders of magnitude greater than the typical annual floods in the receiving rivers (Cenderelli and Wohl, 2001) and some of them can travel >200 km downstream (Richardson & Reynolds, 2000). The extreme
35 discharges, accelerating along the steep mountainous terrains, make GLOFs extremely destructive to downstream communities and infrastructure systems. The unpredictable nature of GLOFs, often occurring without warning, has left downstream communities and infrastructure ill-prepared, causing the loss of human lives and economic damages. The ongoing impact of climate change has introduced additional uncertainty into GLOF risk. The Himalaya region is observing extensive glacier

shrinkage and a proliferation of glacial lakes (Zhang et al., 2015). The potential impacts of GLOFs on downstream communities are expected to intensify further due to population growth and socio-economic development. Hence, it is crucial to develop effective strategies for managing GLOF risks to enhance human safety and support sustainable development. This necessitates the requirement for reproducible assessment of GLOF hazards and their potential impacts arising from these glacial lakes.

Some potentially dangerous lakes have been well-studied individually, such as Tsho Rolpa Lake (e.g., Shrestha & Nakagawa, 2014), Imja Tsho Lake (e.g., Somos-Valenzuela et al., 2015), and Lower Barun Lake (e.g., Sattar et al., 2021). However, these studies provide limited insight into the overall danger and potential impacts of glacial lakes as a whole. While there have been assessments of glacial lake hazards in the Himalayan region, certain limitations exist. Previous work by Mool et al. (2011) and Bajracharya et al. (2020) employed remote sensing techniques to identify potentially dangerous glacial lakes (PDGLs) in Nepal, considering different hazard factors. Rounce et al. (2017) undertook a similar study, quantifying the hazard level of 131 glacial lakes with > 0.1 km^2 area in Nepal. Furthermore, Rounce et al. (2017) evaluated the potential downstream impacts of GLOFs caused by these glacial lakes using a simple flood model without any physical basis. This simple flood model has also been applied to evaluate the overall impacts of GLOFs originating from multiple glacial lakes in the Indian Himalayas (Dubey & Goyal, 2020). Zheng et al. (2021) extended their analysis to assess the impacts of GLOFs across the Third Pole by using a Geographic Information System (GIS)-based hydrological model. However, the complexity of GLOFs renders simple flood models inadequate for capturing their dynamics, thereby making them incapable of supporting detailed assessments of potential impacts on downstream communities and infrastructure.

A range of physically based hydrodynamic models have been developed and applied to predict the spatial-temporal process of GLOFs, offering detailed insights into the resulting flood impacts (e.g., Worni et al., 2014; Ancey et al., 2019; Sattar et al., 2019). Recently, researchers have explored the use of a hydrodynamic model to assess GLOF downstream impacts in the Third Pole (Zhang et al., 2023b). However, hydrodynamic models entail a huge amount of computation and face substantial demands for computation resources when applied at a large scale. What's even more challenging is that the computational requirements increase significantly when addressing GLOF simulations involving a large number of scenarios, which is necessary for assessing GLOF's potential impact due to the complexity and uncertainty of the glacier lake breach process. Moreover, the application of hydrodynamic models to support GLOF modeling and impact assessment necessitates a considerable amount of data, and data availability poses another significant challenge.

The high-alpine conditions have constrained our ability to acquire detailed spatial data for multiple lakes across a large scale. To correctly depict the dynamic inundation process of GLOFs, glacial lake conditions and dam breaching process are essential to estimating the outflow discharge resulting from a breach. While the distribution and changes of glacial lakes have been extensively mapped from increasingly available satellite imagery (e.g., Zhang et al., 2015; Nie et al., 2017; Shugar et al., 2020), accurately determining lake volume and reliably predicting dam breaching processes has remained a challenge because high-alpine conditions impede detailed fieldwork. Combining satellite imagery with existing lake bathymetry measurements offers the possibility of estimating water volumes and peak discharges from outbursts by establishing empirical relationships (e.g., Zhang et al., 2023a). However, estimated lake volumes and potential peak discharges derived from these empirical relationships can vary by up to an order of magnitude (Cook and Quincey, 2015; Muñoz et al., 2020). To account for the uncertainties inherent in conventional empirical relationships, Veh et al. (2020) developed a Bayesian robust regression, utilizing data from the bathymetric survey of 24 glacial lakes. This model estimates water volume based on the surface areas of glacial lakes. Simultaneously, they created a Bayesian variant of a physical dam-break model originally proposed by Walder & O'Connor (1997) to predict peak discharge associated with the estimated flood volume. The Bayesian estimates explore the parameter space of plausible flood volumes and associated peak discharges, generating a million possible outburst scenarios for each lake. These scenarios comprehensively consider all potential conditions of the dam breach process for each specific lake and provide a full range of input information for hydrodynamic models, thereby facilitating predictions of the GLOF

inundation process. Therefore, this study aims to leverage these established Bayesian models to support GLOF inundation simulations.

GLOF exposure and impact assessment are also restricted by data sparsity. Previous studies have typically relied on census data at coarse spatial resolutions or aggregated land use data that encompasses various objects like properties and infrastructure, to estimate the potential socio-economic impact of GLOFs (e.g., Shrestha & Nakagawa, 2014; Rounce et al., 2016). Benefiting from the emergence of new data technologies and the resulting enhancements in data quantity and quality, a spatially explicit assessment method has been developed to identify GLOF exposure at an object level and applied to the Tsho Rolpa Lake (Chen et al., 2022). Employing a similar strategy, essential socio-economic information is collected and processed from various sources, including OpenStreetMap (OSM), Google Earth, global data products, and local archives. The information is used to create a spatial exposure dataset that specifies the locations of different objects, such as individual buildings and hydropower facilities. Subsequently, this spatial exposure data is overlaid with the spatially distributed flood simulation outputs to identify potential exposure to GLOFs along their path.

Overall, this study aims to innovate a framework for object-based exposure and potential impact assessments of GLOFs for multiple lakes across a large scale by exploring the use of remote sensing techniques, the developed Bayesian regression models for estimating lake volumes and potential peak discharges, a physically based hydrodynamic model supported by parallelized high-performance computing, and socio-economic information from multiple sources. Nepal has been chosen as the test area due to its abundance of glacial lakes, and it has been reported to experience the most significant national-level economic consequences from GLOFs globally (Carrivick & Tweed, 2016).

2 Methodology and data

The proposed framework for object-based exposure and impact assessment of GLOFs across multiple lakes comprises several key components: extraction of glacial lake water surfaces from multi-temporal imagery, estimation of lake volumes and peak discharges using well-established Bayesian regression models, utilization of a high-performance hydrodynamic flood model accelerated by graphics processing unit (GPU) technology, and the creation of an exposure dataset sourced from open-source data (Fig. 1). In particular, leveraging multi-temporal imagery availability, a Random Forest model is developed using a set of predictor variables to delineate the maximum extent of glacial lake water surfaces. The plausible range of glacial lake water depths, volumes, and GLOF-induced peak discharges is estimated through existing Bayesian models. A substantial number of GLOF scenarios, encompassing outflow discharge hydrographs through glacial lakes, are sampled and generated based on the plausible range of peak discharges. For each scenario, the resulting outflow discharge hydrograph is employed to drive the GPU-accelerated hydrodynamic model, efficiently simulating the temporal and spatial dynamics of floods. These flood dynamics are then overlaid with the spatial exposure data to identify potential exposure to GLOFs and quantify damage extent by using established depth-damage curves.
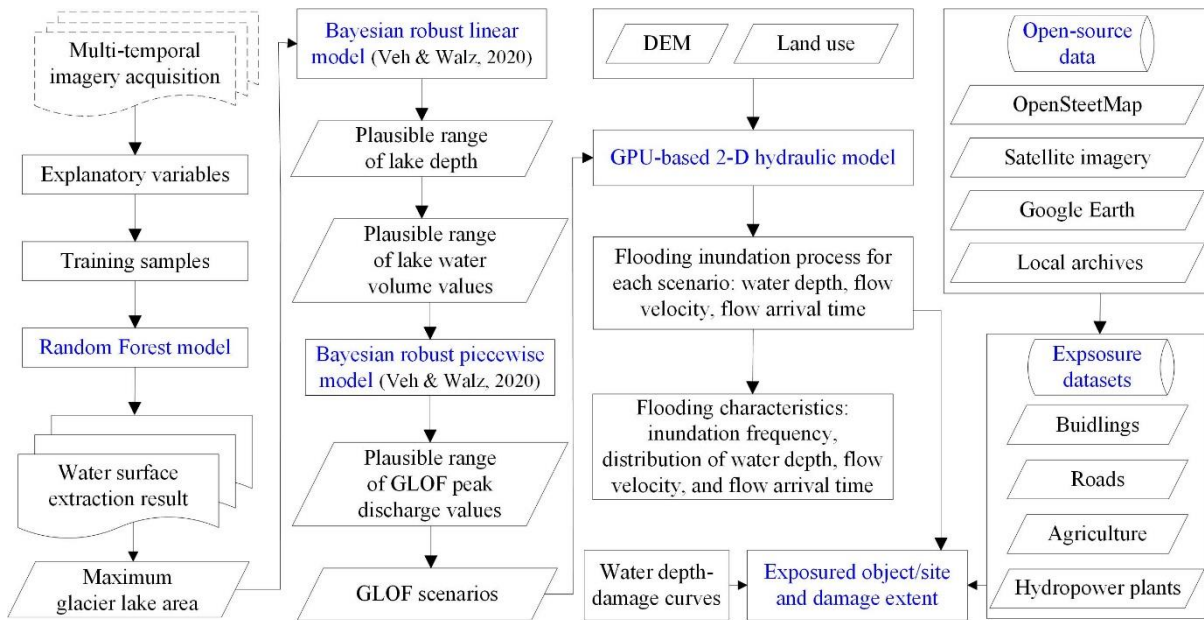
Fig. 1. GLOF exposure and impact assessment framework for multiple glacial lakes (key components highlighted in blue)

2.1 Glacial lake water surface extraction

115   With the availability of multi-temporal imagery, a Random Forest model based on a set of predictor variables is used to map the location and extent of water surfaces of glacial lakes under different hydrological conditions to produce the maximum extent of lake water surfaces.

2.1.1 Acquisition of satellite imagery

Sentinel-2 is an operational multispectral imaging mission of the European Space Agency for global land observation. The

120   Sentinel-2A and -2B satellites were launched in 2015 and 2017, respectively. These satellites capture imagery every 10 days (every 5 days with the twin satellites together). The spatial resolution for the visible and broad near-infrared (NIR) bands is 10m, while it is 20m for the red edge, narrow NIR, and short-wave infrared bands. Here, all available Sentinel-2 imagery for the case study of glacial lakes is utilized to identify the maximum extent of their water surfaces. The analysis is based on the Sentinel-2 level-1C Top-Of-Atmosphere (TOA) products, which are accessible through the Google Earth Engine. Any

125   observations affected by clouds are masked using the Sentinel-2 Quality Assurance band flags. Bands originally at a 20-m resolution are resampled to 10m using the nearest neighbor method before being stacked for subsequent interpretation. All available Sentinel-2 datasets are collected and filtered to reserve imagery from the ablation season, reducing the impact of frozen water surfaces, as per the empirical period of the local melt season (Shugar et al., 2020). In total, 1,520 Sentinel-2 images have been collected for this purpose.

130   2.1.2 Random Forest model

Mapping water surfaces from multiple images is a complex task that necessitates the consideration and analysis of various water-related signals in spectral responses, often influenced by water turbidity and bottom sediments. In this context, a Random Forest model is developed based on a set of predictor variables to extract water surfaces. Random Forest modeling is an ensemble classification technique (Breiman, 2001) and has been extensively used in the classification of remote sensing data

135   (e.g., Yu et al., 2011; Rodriguez-Galiano et al., 2012). Random Forest models excel at recognizing regional variations in threshold values, surpassing the capabilities of traditional index thresholding methods (Tulbure et al., 2016). Notably, Random Forest models do not rely on data distribution assumptions and can yield accurate predictions without overfitting data.

Consequently, they have been increasingly used in water surface extraction as a favorable alternative to traditional statistical approaches (e.g., Schaffer-Smith et al., 2017; Veh et al., 2018).

140 Random Forest model consists of a set of classification trees, each of which grows from a random subset of training samples and randomly permuted explanatory variables. The classification trees can grow to a specified maximum number without pruning, and the final classifications are determined by the majority votes of the trees in the forest. The explanatory variables for Sentinel-2 datasets in the Random Forest model include TOA reflectance for every spectral band, brightness temperature, vegetation indices, and water indices. TOA reflectance and brightness temperature are obtained by normalizing the target

145 imagery, mitigating unwanted effects resulting from variations in sun angle and earth-sun distance. The vegetation indices include the Normalized Difference Vegetation Index (NDVI) and the Enhanced Vegetation Index (EVI). NDVI is sensitive to chlorophyll and used to assess terrestrial vegetation conditions (Tucker, 1979), while EVI is developed to optimize the vegetation signal in high biomass regions, de-couple canopy background signal, and reduce atmospheric influences (Huete et al., 2002). Water indices include the Normalized Difference Water Index (NDWI, McFeeters, 1996), Modified NDWI

150 (MNDWI, Xu, 2006), and Normalized Difference Moisture Index (NDMI, Gao, 1996). NDWI enhances the response to open water features while minimizing soil and terrestrial vegetation influences. MNDWI substitutes the middle infrared band for the NIR band used in the NDWI to enhance water features and remove noise from other land types. NDMI is an effective indicator of vegetation water content. The training samples are selected via visual interpretation of satellite images to represent glacial lake water surfaces, along with various non-water covers, including diverse landscapes and vegetation types. The

155 uncertainty in estimating glacial lake area is quantified using a widely used buffer method (Granshaw and Fountain, 2006). A buffer area of half a pixel (e.g., Zhang et al., 2015; Krause et al., 2019) is adopted to measure the uncertainty in the estimated lake area. The misclassified glacial lake water areas resulting from terrain shadows are eliminated during post-processing through manual exclusion of inaccurately classified regions.

2.2 GLOF dynamic inundation process simulation

160 Using the maximum extent of glacial lake water surfaces, we employ the established Bayesian models to predict glacial lake conditions and the dam breaching process. This allows us to estimate the full range of GLOF outflow discharge through the breach. Subsequently, various GLOF scenarios featuring a range of outflow discharge hydrographs are then sampled to drive the GPU-based hydrodynamic model for the simulation of dynamic flood dynamics resulting from GLOFs.

2.2.1 Estimating volumes and peak discharge of glacial lakes

165 Global samples from glacial lakes have suggested that the water depths for glacial lakes with similar surface areas can vary by one order of magnitude. To estimate water volumes of glacial lakes, we adopted the model that relates lake areas to their maximum depths, which was developed by Veh & Walz (2020). The model was built by compiling the reported lake areas and maximum depths obtained from bathymetric surveys conducted on 24 Himalayan glacial lakes. A Bayesian robust linear regression with a normally distributed target variable (lake depth d) $d \sim N(\mu_d(a), 1/\tau)$ is adopted to account for possible

170 effects of the limited sample size and outliers present in the compiled dataset. The mean $\mu_d(a)$ is calculated below through a linear combination of the input lake area a. The precision τ (the inverse of variance) is gamma-distributed $\tau \sim \Gamma(0.001, \ 0.001)$.

$$\mu_d(a) = \ \alpha_0 + \ \alpha_1 a \tag{1}$$

Where a is lake area, intercept $\alpha_0 \sim N(0, \ 10^{-12})$, slope $\alpha_1 \sim N(0, \ 10^{-12})$.

175 We obtained 100 posterior estimates for the lake depth (d) from the Bayesian model for each lake. For each lake, samples inside the 95% highest density interval (HDI) of credible lake depth values are reserved, i.e., 94 lake depth samples for each

lake. In this study, we maintained the same assumption regarding the bathymetry of the glacial lakes as outlined by Veh & Walz (2020). The delineated lake from satellite imagery is circular, and each lake is assumed to have an ellipsoidal bathymetry. Therefore, we obtained 94 estimates of total volume (V_{tot}) for each glacial lake.

$$V_{tot} = (2/3)\, da \tag{2}$$

With regard to estimating peak discharge during dam failure, Veh & Walz (2020) built a Bayesian piecewise robust model to characterize the physically motivated model developed by Walder & O'Connor (1997). The latter model predicts peak discharge Q_p during natural dam failure. In their study, Walder & O'Connor (1997) compiled data from 63 observed natural dam breaks in various settings and identified a constant response of dimensionless peak discharge $Qp*$ when plotted against the dimensionless product η of lake volume and breach rate k. They inferred a model that describes the relationship between peak discharge and lake volume using the dimensionless peak discharge $Qp*$.

$$Q_p^* = Q_P\, g^{-\frac{1}{2}} h^{-\frac{5}{2}} \tag{3}$$

$$\eta = V_O^* k^* \tag{4}$$

Where $V_O^* = V_0 h^{-3}$ represents the dimensionless flood volume, $k^* = k g^{-1/2} h^{-1/2}$ is the dimensionless breach rate, g is the acceleration of gravity, h is breach depth, and V_0 is the released water volume. k is the breach rate and subsumes lithologic conditions, the erodibility of the outflow channel, and the breach and downstream valley geometry. h is measured from the final lake surface after dam failure to the initial lake surface. V_0 is the released water volume and depends on h and V_{tot}.

Empirical data support a piecewise regression model in the form $Q_p^* = b_0 \eta^{b_1}$ (b_0 and b_1 are the regression parameters) for $\eta < \eta_c$, and Q_p^* is constant for $\eta > \eta_c$. Bayesian piecewise linear regression was developed for predicting peak discharge Q_p^* from η, the product of breach rate k and released flood volume (Veh & Walz, 2020). To account for the most severe GLOFs, we assume that the entire total lake volume V_{tot} would be released to create GLOFs. For each lake, we predicted the peak discharge Q_p based on a given value of V_{tot} and η using the Bayesian piecewise linear regression model. We generated 100 estimates of the posterior predicted Q_p for each given value of V_{tot} and η. The values of η for individual lakes encompass the assumed flood volumes, and we also considered 100 physically plausible values of the breach rate k based on a log-normal fit to reported breach rates. By multiplying the 94 samples of V_{tot} with the 100 samples of k and 100 samples of Q_p, we ultimately obtained a total of 940,000 scenarios of Q_p per lake. Considering the substantial computational resources required for GLOF inundation simulations in Section 2.2.2, 1,000 scenarios are randomly selected from the total of 940,000 Q_p scenarios per lake. The weight of each scenario is determined by its occurrence probability, specifically, the proportion of times its peak discharge does not exceed that of other scenarios, relative to the total number of scenarios. A smaller proportion indicates a lower likelihood of occurrence, while a larger proportion indicates a higher likelihood. The weight of each scenario is calculated by dividing the proportion by the total proportion of all possible scenarios. In these simulations, the dam breach hydrograph is assumed to have an isosceles triangle shape, simplifying its derivation from Q_p and V_0. The breach hydrograph then serves as the boundary condition for the hydrodynamic modeling. Although there is some uncertainty, the assumption of an isosceles triangle shape for the dam breach hydrograph aligns with experimental observations (e.g., Morris et al., 2007; Walder et al., 2015; Yang et al., 2015) and is supported by simulation results from commonly used mechanisms and empirical models (e.g., Yang et al., 2023). Apart from the most severe scenarios, less severe conditions are also considered, where 25%, 50%, and 75% of the lake water volume are released.

2.2.2 2-D hydrodynamic modeling

The High-Performance Integrated Hydrodynamic Modelling System (HiPIMS) (Zhao & Liang, 2022) is employed here to simulate the breach hydrograph. HiPIMS develops a fully dynamic model based on the 2-D depth-averaged shallow water equations. The conservative form of the governing 2-D shallow water equations is expressed as follows:

$$\frac{\partial \mathbf{q}}{\partial t} + \frac{\partial \mathbf{f}}{\partial x} + \frac{\partial \mathbf{g}}{\partial y} = \mathbf{s} \tag{5}$$

where t is the time; x and y represent the Cartesian coordinates; $\mathbf{q}$ denotes the flow variable vector; $\mathbf{f}$ and $\mathbf{g}$ are the flux vectors in the x- and y-direction, respectively; and $\mathbf{s}$ is the source term vector. The vector terms are defined as:

$$\mathbf{q} = \begin{bmatrix} h \\ q_x \\ q_y \end{bmatrix} \qquad \mathbf{f} = \begin{bmatrix} q_x \\ uq_x + \frac{1}{2}gh^2 \\ uq_y \end{bmatrix}$$

$$\mathbf{g} = \begin{bmatrix} q_y \\ vq_x \\ vq_y + \frac{1}{2}gh^2 \end{bmatrix} \qquad \mathbf{s} = \begin{bmatrix} 0 \\ -C_f u\sqrt{u^2 + v^2} - gh\frac{\partial z_b}{\partial x} \\ -C_f v\sqrt{u^2 + v^2} - gh\frac{\partial z_b}{\partial y} \end{bmatrix} \tag{6}$$

where h is the water depth; $q_x = uh$ and $q_y = vh$ are the unit-width discharges in the x- and y- directions, respectively; u and v denote the depth-averaged velocities in two Cartesian directions; and z_b is the bed elevation; and C_f is the bed roughness coefficient.

The governing equations outlined above are solved through a shock-capturing finite volume Godunov-type scheme on uniform grids (Zhao & Liang, 2022). The numerical scheme introduces a robust Godunov-type model to deliver precise and stable predictions of overland flow and flooding processes at the catchment scale. This scheme is implemented through a Python and CUDA C hybrid programming framework to achieve multi-GPU and multi-node high-performance computing for large-scale simulations. It's worth noting that the GPU-accelerated model has demonstrated computational efficiency up to ten times greater than its CPU-based counterpart (Smith & Liang, 2013). HiPIMS is set up using the terrain data and roughness data, and it is driven by the breach hydrograph for each scenario, as calculated in Section 2.2.1. Subsequently, the runoff is automatically routed throughout the flow area.

2.3 GLOF exposure and impact assessment

Based on the GLOF inundation process predicted by HiPIMS for each scenario, which includes water depth, flow velocities, and flood arrival time, we can estimate potential flood exposure by superimposing the exposure datasets onto the flood simulation results. In addition to assessing flood exposure, it is imperative to quantify the potential losses and impacts of GLOFs under various conditions to understand the associated risks. Estimating the direct damage to buildings and other exposed objects can be achieved by employing appropriate depth-damage curves that establish the relationship between flood depth and the potential damage. Typically, the damage is quantified as a percentage of the cost required for repairs or replacements. In this study, we utilize depth-damage curves from the HAZUS Flood model to investigate the impact of GLOFs on buildings (Scawthorn et al., 2006). Beyond buildings, GLOFs can also have a significant impact on agricultural lands and roads. We evaluate the damage to agricultural lands and roads caused by GLOFs using the damage curves recommended in a technical report published by the Joint Research Centre of the European Commission (Huizinga et al., 2017). The specific water depth-damage curves for buildings, roads, and agricultural lands used in this study can be referenced in Chen et al. (2022).

2.4 Data

HiPIMS is set up using a digital elevation model (DEM) to represent domain topography and land use data to parameterize domain roughness. It is driven by the out-of-breach flow discharge estimated in Section 2.2.1. The DEM used in this work is Shuttle Radar Topography Mission (SRTM) DEM with a spatial resolution of 30 m (Farr et al., 2007). Land use types are extracted from the Landsat Thematic Mapper imagery from the year 2010, provided by the International Centre for Integrated Mountain Development (ICIMOD, 2020). The roughness of the flow area is represented by the Manning coefficient (n), which is dependent on land use types. The values assigned are 0.15 for forest, 0.035 for arable land, 0.03 for grassland, 0.027 for water surface, and 0.016 for construction land. The Manning coefficients 0.016 to 0.15 were specified based on values provided in earlier hydraulic textbooks or reports (such as Chow, 1959; Barnes, 1967; Arcement and Schneider, 1984), aligning with previous studies, for example, 0.035 to 0.17 in Nepal (Sattar et al., 2021) and 0.035 to 0.120 in Bhutan (Rinzin et al., 2023).

Open-source datasets are used to support the assessment of GLOF exposure and impacts. The OSM is a collaborative user-generated project initiated in 2004 to provide an openly available geographical database of the world, covering both the natural and artificial environments of the Earth's surface (OpenStreetMap contributors, 2015). While primarily built by volunteers, OSM also integrates geographical data contributed by governmental and specialized GIS databases for certain areas or entire countries, e.g., Nepal, providing relatively complete spatial data on buildings and other objects. Hydropower plant data are obtained from the Hydro Map project (Nepal Hydropower Portal, 2019). In the Hydro Map project, hydropower plants are categorized into three types: operation, generation, and survey. In Nepal, the hydropower licensing regime is divided into two stages i.e., a survey license is issued to conduct a feasibility and environmental assessment, and a generation license is granted after the project is found to be technically, environmentally, and economically viable. Detailed information on each hydropower plant is provided, including its province, district, local Government, capacity, commission/issue date, longitude, latitude, etc. Importing hydropower plant data in ArcGIS and comparing it with sub-meter imagery from ArcGIS Server and Google Earth, the positions of some hydropower plants are found to be inaccurate. To address the inaccuracies in the positions of some hydropower plants, a process has been undertaken to enhance the quality of the hydropower plant data. The coordinates of existing hydropower plants, including those in operation and under construction, have been collected from Wikipedia. These coordinates are then visually inspected and collected against sub-meter imagery obtained from ArcGIS Server and Google Earth, as they are discernible in sub-meter imagery. The newly collected coordinates will be utilized to update the spatial positions of hydropower plants provided by the Hydro Map project.

3 Study area and glacial lakes

Nepal is highly vulnerable to GLOFs. A total of 53 GLOF events have been documented in Nepal from 1560 to now (Shrestha et al., 2023). Additionally, there have been 37 GLOF events recorded in the Tibetan Autonomous Region, China, that had transboundary impacts on Nepal. These historical events have had devastating consequences for the country. For example, both the 1985 Dig Tsho GLOF and the 1998 Tam Pokhari GLOF had devastating effects, resulting in significant loss of life, property and infrastructure damage, and severe disruptions to the livelihoods of those living in downstream areas. Approximately 1.56 million people live downstream within 3 km of moraine-dammed lakes in Nepal, putting them at risk of GLOFs (Ghimire, 2004). If climate change continues at its present pace, rates of glacier mass loss and shrinkage and the formation and expansion of glacial lakes will increase further, which could escalate the occurrence of GLOFs. Exacerbating the situation, GLOF exposure and risk are on the rise due to the expansion of settlements, economic activities, and infrastructure construction along riverbanks.

In Nepal, a total of 2,070 glacial lakes with lake areas equal to or larger than 0.003 km^2 have been identified and mapped using Landsat images (Bajracharya et al., 2020). These glacial lakes are predominantly situated in northern Nepal, at elevations

ranging from 3400m to 5908m. Notably, 98% of these glacial lakes are positioned above 4000m. Bajracharya et al. (2020) assessed GLOF hazard factors related to lake and dam characteristics, glacier activity at the source, and the morphology of the lake surroundings for the 2,070 glacial lakes. They identified 21 lakes as PDGLs (Fig 2 and Table 1). Among the 21 PDGLs, some lakes have names, while others do not and were designated as 'Anonymous'. These 21 PDGLs are further categorized 290 into three ranks based on the level of danger associated with GLOF hazards, with Rank I representing the highest level of risk.
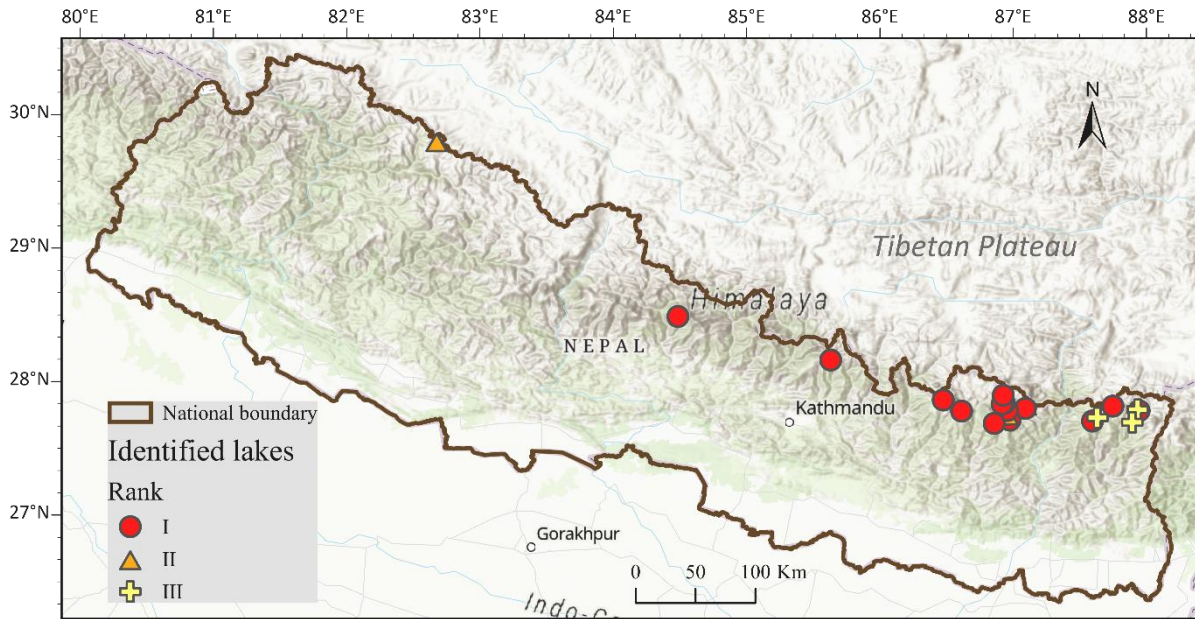
Fig 2. Study area, and 21 identified dangerous glacial lakes and their danger level rank of GLOF hazards with Rank I being the highest.

In this study, the focus is on these 21 PDGLs, and a comprehensive assessment of their GLOF risk and downstream impacts 295 is conducted. Each lake is assessed using the proposed evaluation framework in Section 2. The model and evaluation domain for each lake are determined based on the maximum potential inundation extent resulting from GLOFs, as well as the topographic features and river network conditions downstream. Typically, the domain spans more than 100 km and is sufficiently extensive to encompass all potential impacts.

Table 1 Delineated glacial lake areas under varied water-occurrence frequency from multi-temporal Sentinel-2 imagery

Lake number	Lake ID	Lake name	Longitude (E)	Latitude (N)	Rank	Area (km^2) (> 5%)	Area (km^2) (> 25%)	Area (km^2) (> 50%)
1	GL087749E27816N	Anonymous 1	87°44′59″	27°48′57″	I	0.178 ± 0.011	0.169 ± 0.011	0.161 ± 0.011
2	GL087934E27790N	Anonymous 2	87°56′05″	27°47′26″	III	0.148 ± 0.012	0.134 ± 0.012	0.112 ± 0.010
3	GL087945E27781N	Anonymous 3	87°56′42″	27°46′51″	I	0.048 ± 0.005	0.040 ± 0.005	0.035 ± 0.004
4	GL087632E27729N	Anonymous 4	87°37′55″	27°43′44″	III	0.036 ± 0.004	0.032 ± 0.004	0.016 ± 0.005
5	GL087596E27705N	Anonymous 5	87°35′46″	27°42′18″	I	0.026 ± 0.003	0.020 ± 0.003	0.010 ± 0.003
6	GL087893E27694N	Anonymous 6	87°53′36″	27°41′41″	III	0.037 ± 0.005	0.028 ± 0.005	0.015 ± 0.004
7	GL086925E27898N	Imja Tsho	86°55′30″	27°53′53″	I	1.741 ± 0.047	1.630 ± 0.042	1.561 ± 0.041
8	GL086476E27861N	Tsho Rolpa	86°28′34″	27°51′40″	I	1.712 ± 0.043	1.657 ± 0.041	1.610 ± 0.040
9	GL086928E27850N	Anonymous 7	86°55′41″	27°51′00″	I	0.553 ± 0.021	0.533 ± 0.021	0.510 ± 0.022
10	GL086935E27838N	Hongu 1	86°56′06″	27°50′17″	I	0.322 ± 0.018	0.305 ± 0.018	0.293 ± 0.018
11	GL086917E27832N	Anonymous 8	86°55′01″	27°49′55″	I	0.361 ± 0.015	0.342 ± 0.014	0.332 ± 0.014
12	GL087095E27829N	Anonymous 9	87°05′42″	27°49′44″	II	0.118 ± 0.008	0.114 ± 0.008	0.037 ± 0.012
13	GL087092E27798N	Lower Barun	87°05′31″	27°47′53″	I	2.193 ± 0.048	2.044 ± 0.046	1.900 ± 0.053
14	GL086957E27783N	Hongu 2	87°57′25″	27°46′59″	I	0.872 ± 0.030	0.865 ± 0.030	0.843 ± 0.030
15	GL086612E27779N	Lumding	86°36′43″	27°46′44″	I	1.475 ± 0.037	1.411 ± 0.034	1.349 ± 0.035
16	GL086958E27755N	Chamlang	86°57′29″	27°45′18″	II	0.921 ± 0.027	0.856 ± 0.021	0.700 ± 0.026
17	GL086977E27711N	Anonymous 10	86°58′37″	27°42′40″	I	0.085 ± 0.007	0.074 ± 0.007	0.009 ± 0.003
18	GL086858E27687N	Anonymous 11	86°51′29″	27°41′13″	I	0.336 ± 0.015	0.324 ± 0.015	0.307 ± 0.014
19	GL085630E28162N	Anonymous 12	85°37′51″	28°09′44″	I	0.150 ± 0.009	0.137 ± 0.008	0.124 ± 0.008
20	GL082673E29802N	Anonymous 13	82°40′27″	29°48′09″	II	0.047 ± 0.006	0.041 ± 0.005	0.032 ± 0.005
21	GL084485E28488N	Thulagi	84°29′06″	28°29′17″	I	0.997 ± 0.032	0.964 ± 0.032	0.921 ± 0.029

300

4 Results

4.1 Glacial Lake Water Surface Extraction

Water surfaces of glacial lakes are delineated from Sentinel-2 images using the Random Forest model, as previously outlined. The Random Forest model is trained with a set of training samples that comprise both water and non-water features. To account for seasonal variations in lake water surfaces, the training samples for water features are manually selected from images acquired at different times. Various non-water features encompass diverse landscapes and vegetation types. This training dataset is subsequently employed to drive and train the Random Forest model, which is then employed to delineate water surfaces for all the adopted Sentinel-2 images. The subsequent analysis involves the computation of water-occurrence frequency based on multi-temporal water surfaces. The outcomes of water-occurrence frequency for specific representative lakes are visually presented in Fig. 3. It is noteworthy that lake areas are not consistently characterized by open water throughout the year. For instance, lake 'Anonymous 1' (87°44′59″ E, 27°48′57″ N) (Fig. 3(b)) exhibits an average water-occurrence frequency of 72%, while lake 'Anonymous 2' (87°56′05″ E, 27°47′26″ N) (Fig. 3(d)) has an average water-occurrence frequency of 58%. In contrast, for certain lakes, like 'Anonymous 8' (86°55′01″ E, 27°49′55″ N) and the Tsho Ropla Lake, lake areas are always covered with water. Hence, the capacity to map glacial lakes to assess the associated GLOF risk is influenced by the timing of image acquisition.

Table 1 presents the determined lake areas based on varying water-occurrence frequencies. To mitigate the effects of misinterpretations, such as cloud shadows, a 5% threshold is utilized to exclude areas characterized by low water-occurrence frequencies. Subsequently, the maximum lake boundary is delineated for each lake, allowing for the straightforward calculation of maximum lake areas. Among the 21 lakes, the largest one is Lower Barun Lake, a substantial glacial lake in Nepal known for its depth and size. Its area measures 2.193 ± 0.048 km^2, while the smallest lake (Anonymous 5; 87°35′46″ E, 27°42′18″ N) covers only 0.026 ± 0.003 km^2. Lower Barun Lake, along with the second largest PDGL, Imja Tsho Lake, has undergone significant area growth. The estimated maximum area of Imja Tsho Lake here is 1.741 ± 0.047 km^2. Tsho Rolpa Lake boasts a maximum area estimated at 1.712 ± 0.043 km^2. This aligns with previous findings, which reported that the lake had an area of 0.23 km^2 in 1957, which grew to 1.02 km^2 in 1979, 1.65 km^2 in 1999, and 1.61 km^2 in 2019 (Chen et al., 2021). Lumding Lake, another PDGL with an estimated area exceeding 1 km^2, displayed notable growth. It had an area of 0.104 km^2 in 1963, 0.66 km^2 in 1987, 0.8 km^2 in 1996, and 1.18 km^2 in 2016 (Khadka et al., 2019). Our assessment indicates that the maximum area of Lumding Lake is 1.475 ± 0.037 km^2. In summary, the estimated maximum lake areas derived from multi-temporal satellite images for these extensively studied lakes are in good agreement with previous research. To establish the maximum lake boundary for potential risk assessment, it is imperative to leverage multi-temporal imagery capturing various hydrological conditions of glacial lakes.

The maximum areas of the four large lakes (Lower Barun, Imja Tsho, Tsho Rolpa, and Lumding), each exceeding 1 km^2, are approximately 1.1 times the extent to which water covers more than 50% of the time. In contrast, for the comparatively smaller lakes (Anonymous 3, 4, 5, 6, 10, and 13), the ratio of maximum area to the area covered by water for more than 50% of the time can be as high as 1.4 to 2.5 times. For instance, 'Anonymous 10' (86°58′37″ E, 27°42′40″ N) has a maximum area of 0.085 km^2, while only 0.009 km^2 is covered with water for more than 50% of the time. The areas of small PDGLs exhibit more significant variations in space and time compared to those of larger PDGLs, making the associated risks more uncertain. Additionally, the ratio of maximum area to the area covered by water for more than 50% of the time is predominantly in the range of 1.1 to 1.5 for PDGLs with high hazard level I. However, for PDGLs with lower hazard levels II and III, this ratio varies from 1.3 to 3.2. This indicates that the areas of PDGLs with a high hazard level exhibit more stability in terms of space and time compared to those with lower hazard levels.
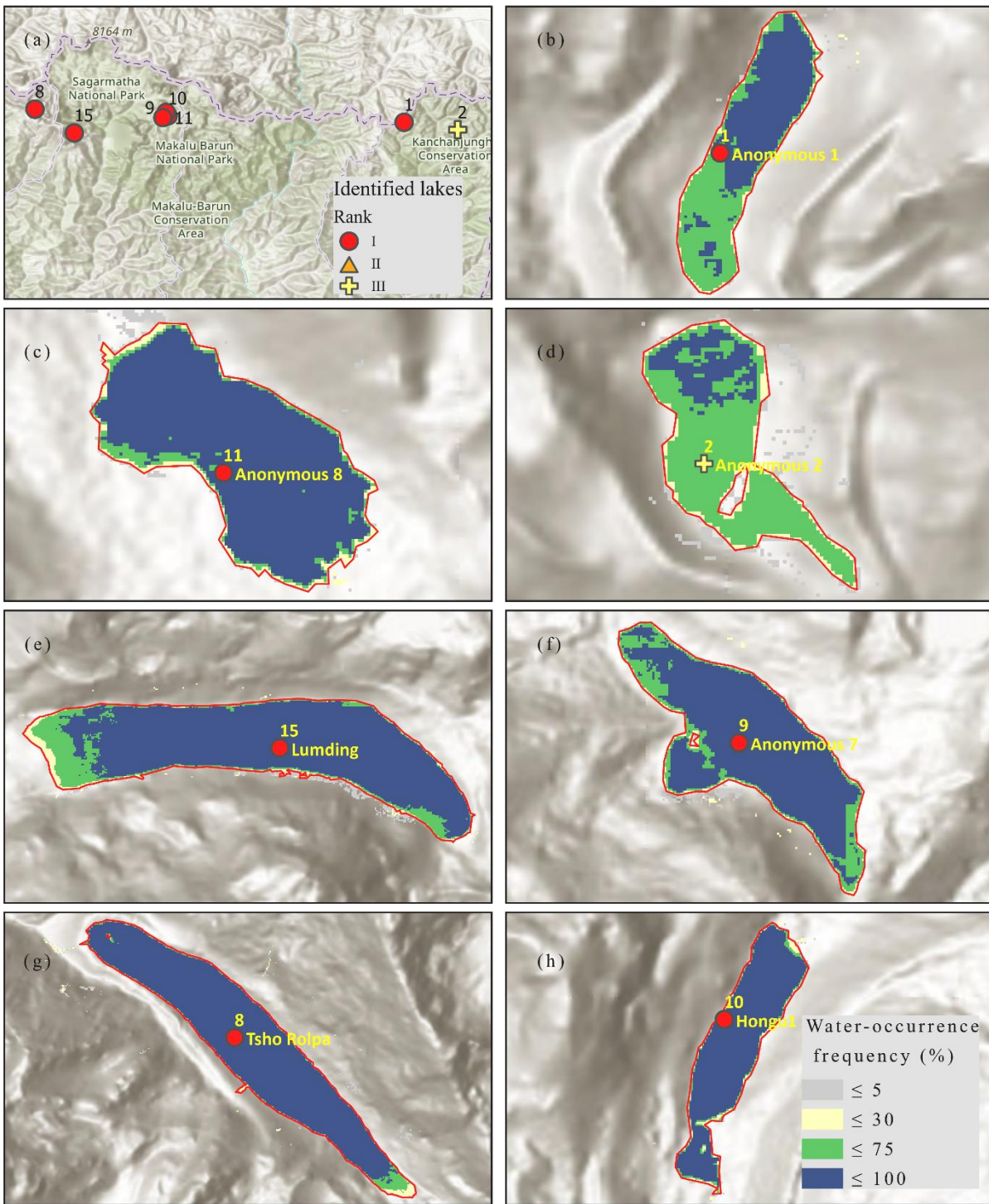
Fig 3 Water surfaces extracted from multi-temporal Sentinel-2 imagery in representative glacial lakes in Nepal (lake numbers and other lake details can be found in Table 1)

4.2 Lake volumes and peak discharges prediction

345   We obtained 94 estimates of the total volume V_{tot} for each lake (Fig 4 (a)) and a total of 940,000 scenarios of peak discharge Q_p per lake (Fig 4 (b)) using the models introduced in Section 2.2.1. The average lake volumes and peak discharges of the 21 PDGLs span more than 2 and 3 orders of magnitude. We collected geophysical investigation data for named PDGLs and compared them against calculated volumes using field-investigated lake areas, as shown in Table 2. While there are some inconsistencies, the calculated volumes generally align with the investigated values. For example, the Lower Barun glacial

350   lake has an average estimated flood volume of 238.9×10^6 m³ and an average estimated peak discharge of 18,240 m³/s. The water volume of the Lower Barun glacial lake in 2015 was approximately 112.3×10^6 m³, with a lake area of 1.52 km² based

on bathymetric measurements. Using the established relationship between lake area and volume, the average volume for a lake with a 1.52 km^2 area is calculated to be 108.27 × 10^6 m^3, which closely matches the measured volume of the Lower Barun glacial lake. For the smallest lake (Anonymous 5) among these 21 PDGLs, its average volume and peak discharge are 0.22 × 10^6 m^3 and 167 m^3/s, respectively. This means that the average volume and peak discharge of the Lower Barun glacial lake are 1,041 and 108 times greater than those of the smallest lake, respectively.
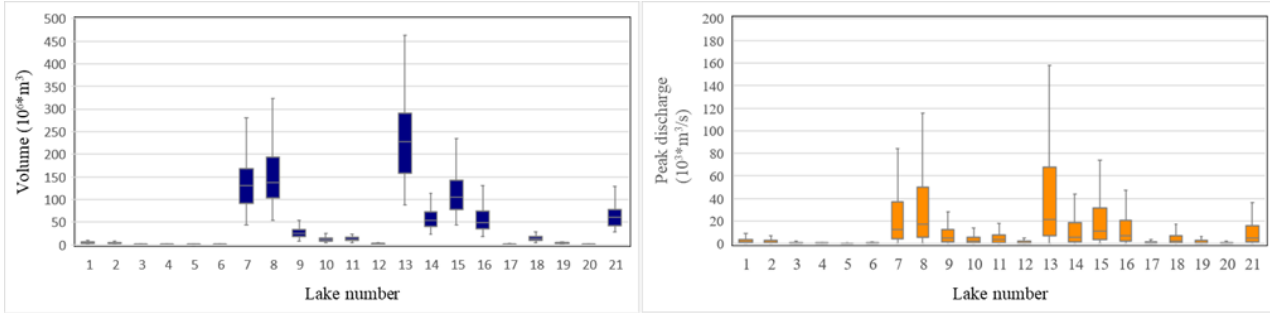
Fig 4 (a) Estimated lake volumes and (b) estimated peak discharges for each glacial lake

Table 2 Comparisons between the lake areas (km^2) and volumes (10^6*m^3) derived from bathymetric investigations and those calculated in this study for named lakes.

Lake number	Lake name	Maximum areas	Estimated volume	Investigation year	Investigated areas	Investigated volume	Calculated volume for the investigated areas	Reference
7	Imja Tsho	1.741	131.16	2016	1.35	88	87.57	Lala et al., (2017)
8	Tsho Rolpa	1.712	138.39	1994	1.39	76.45	92.11	Rana et al., (2000)
13	Lower Barun	2.193	238.86	2015	1.52	112.3	108.27	Haritashya et al., (2018)
15	Lumding	1.475	103.16	2015	1.13	57.7	65.93	Rounce et al., (2016)
16	Chamlang	0.921	49.53	2009	0.87	34.9 - 35.6	45.75	Lamsal et al., (2016)
21	Thulagi	0.997	59.69	2017	0.89	36	47.12	Haritashya et al., (2018)

360

4.3 Flood inundation simulation

4.3.1 Inundation areas

HiPIMS is used to simulate flood dynamics in 1,000 scenarios for each lake with all the lake water volume released. The final flood inundation probability and maximum water depth are derived from each scenario's results multiplied by their respective weight. Herein, we use the simulation results from Imja Tsho Lake and Lower Barun Lake as illustrative examples (Fig. 5). The areas with high flood inundation probabilities are predominantly distributed along the downstream valley. The areas with flood inundation frequency exceeding 50% can be substantial, reaching 51.2 km^2 for Lower Barun Lake and 65.3 km^2 for Lower Barun Lake. The maximum water depth offers spatial insights into the potential severity of GLOFs in downstream areas (Fig. 5(c) and 5(d)). It facilitates the identification of areas characterized by both high inundation probability and significant maximum water depth. For instance, concerning Lower Barun Lake, there are 6.1 km^2 of areas exhibiting both inundation frequency exceeding 90% and maximum water depth exceeding 1m. These specific areas should undoubtedly receive heightened attention in future flood risk management and mitigation.
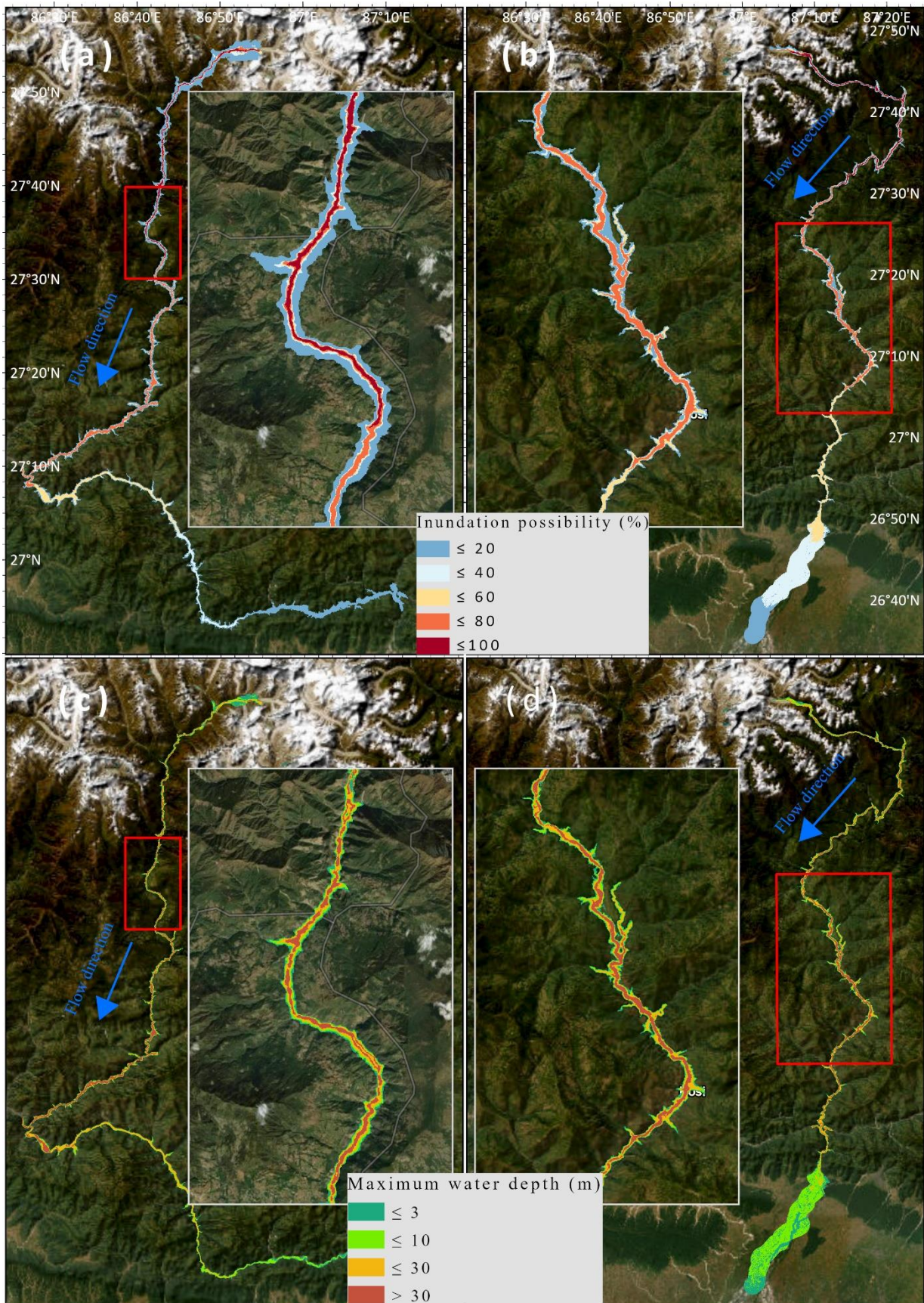
Fig 5 GLOF inundation probability for (a) Imja Tsho Lake and (b) Lower Barun Lake, and maximum water depth for (c) Imja Tsho Lake and (d) Lower Barun Lake under respective worst situation i.e., all lake water will be released. (The basemaps used were accessed from ArcGIS Online Basemap provided by Esri.)

The resulting inundation areas at different levels of inundation probabilities are shown in Fig. 6. The inundation extent resulting from GLOFs originating from the 21 PDGLs ranges from 2.8 km^2 to 190.3 km^2. Notably, the largest glacial lake, Lower Barun

(lake number 13), has an inundation area of 18.2 km² and 65.3 km² for inundation probabilities exceeding 75% and 50%, respectively. Tsho Rolpa Lake (lake number 8), despite having a smaller lake area than Lower Barun, projects inundation areas of 27.6 km² and 78.3 km² for probabilities exceeding 75% and 50%, respectively. Imja Tsho Lake (lake number 7), similar in size to Tsho Rolpa Lake, anticipates inundation areas of 15.8 km² and 51.2 km² for probabilities exceeding 75% and 50%, respectively. It's worth noting that lakes that have not been extensively studied can potentially cause large inundation areas of over 10 km² for probabilities exceeding 50%, including Anonymous 7 (86°55′41″ E, 27°51′00″ N), Anonymous 11 (86°51′29″ E, 27°41′13″ N), Anonymous 12 (85°37′51″ E, 28°09′44″ N), Anonymous 1 (87°44′59″ E, 27°48′57″ N), and Anonymous 2 (87°56′05″ E, 27°47′26″ N). The smallest lake, Anonymous 5 (87°35′46″ E, 27°42′18″ N), has an inundation area of 2.5 km² for probabilities exceeding 50%.
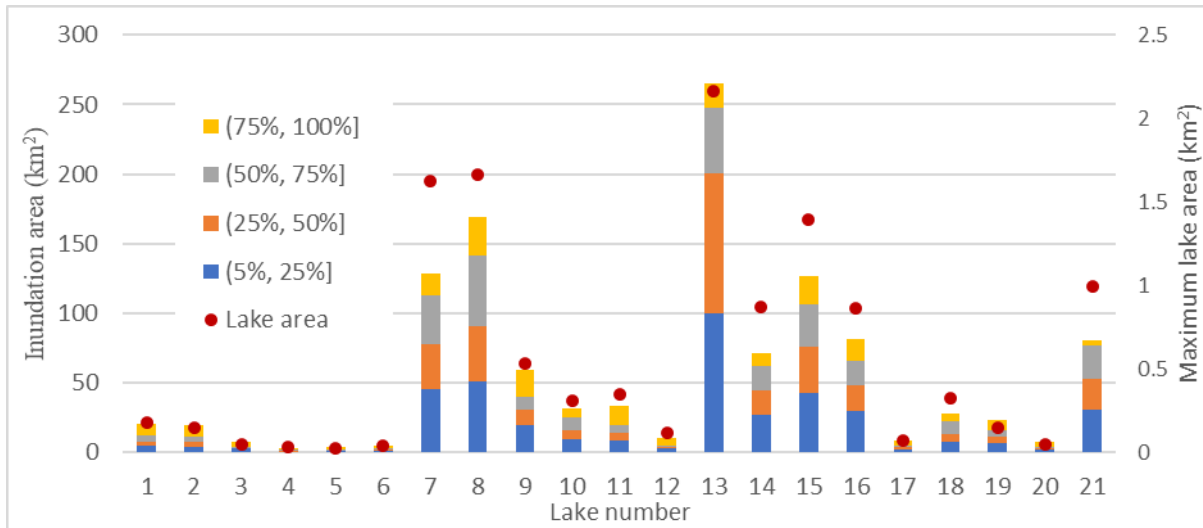
Fig 6 Inundation area (km²) at different levels of inundation probabilities and maximum lake area (km²)

To account for all possible glacial lake outburst scenarios, less severe conditions are also considered, where 25%, 50%, and 75% of the lake water volume is released. In each of these less severe scenarios, 100 cases are randomly selected from a total of 940,000 samples. The outcomes of these scenarios will be compared to the worst-case conditions. Fig 7 illustrates the inundation area for inundation probabilities exceeding 50% resulting from GLOFs. In the case of Lower Barun Lake, the release of 25% and 50% of the lake water leads to the inundation of 50.2 km² and 60.6 km² of downstream areas, respectively. When 100% of the lake water is released, the inundation areas are 1.29 and 1.08 times larger than those under the 25% and 50% lake water release scenarios, respectively. Following Lower Barun Lake, Tsho Rolpa Lake, and Lumding Lake have the potential to cause significant inundation areas. Even with just 25% of the lake water being released, Tsho Rolpa Lake and Imja Tsho Lake can potentially submerge approximately 30 km² of areas with inundation probabilities exceeding 50%.
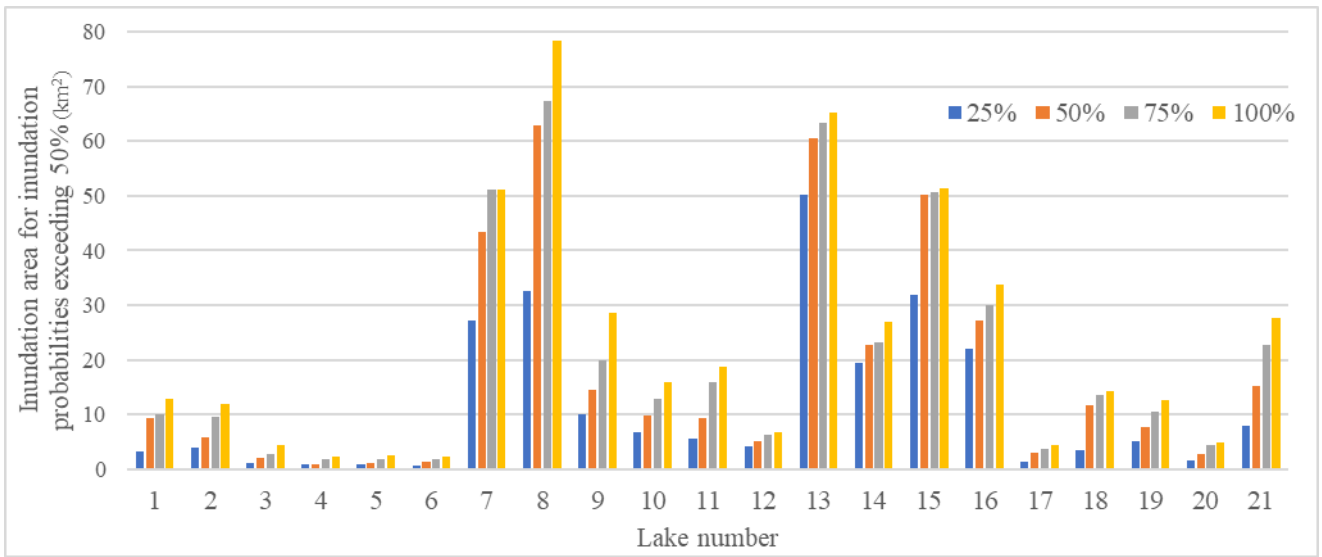
400   **Fig 7 Inundation area (km^2) for inundation probabilities exceeding 50% under 25%, 50%, 75% and 100% of lake water volume released**

Table 3 GLOF induced inundation areas and damage extents to buildings, roads, and agricultural lands

Lake name	Area for inundation probabilities > 50% (km²)	Building number			Building area (m²)			Road (km)			Agriculture land (km²)		
		Slight	Moderate	Substantial	Slight	Moderate	Substantial	Slight	Moderate	Substantial	Slight	Moderate	Substantial
Anonymous 1	12.8	67	174	41	4024	10196	1956	10	6	51	0.7	0.8	6.3
Anonymous 2	11.8	45	127	46	2667	7451	2826	10	5	47	0.8	0.8	4.9
Anonymous 3	4.3	7	22	13	568	1659	850	10	4	17	0.5	0.1	0.1
Anonymous 4	2.3	2	14	4	88	685	151	3	1	10	0.0	0.0	0.0
Anonymous 5	2.5	4	12	2	177	553	107	2	1	2	0.0	0.0	0.0
Anonymous 6	2.3	4	4	2	376	186	58	7	2	12	0.4	0.1	0.2
Imja Tsho	51.2	23	1065	1212	1515	60485	70887	8	25	260	0.1	3.8	40.0
Tsho Rolpa	78.4	26	2236	7126	1256	118002	395563	9	37	675	0.2	4.9	77.5
Anonymous 7	28.6	66	420	179	2651	16272	10082	13	13	67	0.9	2.5	13.0
Hongu 1	15.8	11	178	14	326	10169	304	5	5	33	0.6	1.1	7.1
Anonymous 8	18.7	13	171	17	549	9670	527	5	4	33	0.7	0.9	7.1
Anonymous 9	6.6	2	5	1	72	273	66	5	2	17	0.2	0.1	0.3
Lower Barun	65.3	247	3760	1338	13154	294755	71193	17	22	362	0.4	3.9	76.5
Hongu 2	26.9	47	537	300	1582	19704	15372	12	18	109	0.6	3.2	20.7
Lumding	51.3	2	1141	986	65	46523	41105	6	19	237	0.1	3.9	45.4
Chamling	33.8	12	653	443	368	24815	20706	8	21	141	0.3	3.4	25.7
Anonymous 10	4.4	0	5	5	0	94	82	1	0	1	0.3	0.2	0.4
Anonymous 11	14.3	34	170	28	1434	10405	1086	5	4	31	0.6	1.0	8.2
Anonymous 12	12.6	379	829	174	44635	71601	15516	27	15	67	1.9	1.8	4.7
Anonymous 13	4.8	6	18	0	268	1076	0	12	4	9	0.0	0.0	0.0
Thulagi	27.7	324	6203	2714	23275	488010	216987	39	52	328	1.8	5.6	37.1

4.3.2 Exposure assessment

The exposure of objects can be spatially determined by overlaying the predicted flood inundation maps with relevant datasets detailing buildings, roads, and agricultural land (Table 3). Here, we focus on areas with flood probabilities greater than 50%. The number of inundated buildings varies from 0 to 9,388. Out of the 21 PDGLs, 14 lakes have a number of inundated buildings exceeding 100, while 7 of them inundate at least 1,000 buildings. The three lakes with the highest number of inundated buildings are Tsho Rolpa, Thulagi, and Lower Barun, each of which could inundate more than 5,000 buildings and cover an area of 3.7 * 10^5 m² of building areas. The number of buildings inundated by Tsho Rolpa and Thulagi each is almost twice that of Lower Barun Lake. Overall, these well-studied lakes could impact more buildings than anonymous lakes. These 13 anonymous lakes typically affect fewer than 300 buildings, with the exceptions being Anonymous 7 (86°55′41″ E, 27°51′00″ N) and Anonymous 12 (85°37′51″ E, 28°09′44″ N), which can influence 665 and 1382 buildings, respectively. Further investigation and research are required for the two anonymous lakes. Conversely, three lakes, including Anonymous 10 (86°58′37″ E, 27°42′40″ N), Anonymous 6 (87°53′36″ E, 27°41′41″ N), and Anonymous 9 (87°05′42″ E, 27°49′44″ N), pose lower risks, with a number of 10 or fewer buildings affected.

Regarding inundated roads, the value ranges from 2 to 721 km. Tsho Rolpa Lake, Thulagi Lake, and Lower Barun Lake still hold the top three positions with the largest lengths of inundated roads, each exceeding 400 km. To illustrate, Tsho Rolpa Lake, the top one in this category, inundates a 721 km long road. Following closely is Thulagi Lake, which has inundated roads with a length of 419 km. Agriculture is a cornerstone of the Nepalese economy, and it is susceptible to the impacts of GLOFs. It is anticipated that eight lakes have more than 10 km² of inundated agricultural land, while three lakes have a negligible impact on agriculture. Tsho Rolpa Lake, Lower Barun Lake, and Lumding Lake are the most perilous lakes concerning the inundation of agricultural lands.

In addition to the high potential for human settlements to be exposed to GLOFs, hydropower projects are increasingly vulnerable to these events. Hydropower development in Nepal has grown rapidly but unevenly. This development trend involves projects moving upstream, bringing hydropower plants closer to glacial lakes. According to the hydropower development data collected in the Hydro Map project (Niti Foundation, n.d.), Nepal has a total of 572 hydropower projects. These projects include 81 that are currently operational, 180 with issued generation licenses, and 311 with issued survey licenses. Among these, 12 existing hydropower plants (including those in operation and under construction; Table 4) are situated close to GLOF flow channels and are potentially at risk from GLOFs due to 21 PDGLs. The 12 hydropower plants facing such risks are Khimti I, Upper Tamakoshi, Chatara, Devighat, Trishuli, Marsyangdi, Middle Marsyangdi, Upper Marsyangdi A, Tallo Khare Khola, Arun III, Upper Trishuli-1, and Middle Tamor. Additionally, 38 hydropower plants, for which generation or survey licenses have been issued, are also exposed to the risk of GLOFs from these 21 PDGLs. These hydropower plants deserve increased attention in future GLOF risk management due to their significant importance and high vulnerability. Specifically focusing on certain lakes, Tsho Rolpa, Thulagi, and Lower Barun are responsible for potentially inundating 6 plants (3 existing and 3 with licenses), 6 plants (3 existing and 3 with licenses), and 5 plants (2 existing and 3 with licenses), respectively. Furthermore, Lumding and Imja Tsho can each impact 4 hydropower plants with licenses. Surprisingly, lakes Anonymous 12 (85°37′51″ E, 28°09′44″ N), Anonymous 1 (87°44′59″ E, 27°48′57″ N), and Anonymous 2 (87°56′05″ E, 27°47′26″ N) have the potential to cause the inundation of 10 plants (3 existing and 7 with licenses), 8 plants (1 existing and 7 with licenses), and 6 plants (1 existing and 5 with licenses), respectively.

Table 4 GLOF induced inundation hydropower plants

Hydropower plant	State	Lake name
Khimti I	Operation	Tsho Rolpa
Upper Tamakoshi	Operation	Tsho Rolpa

Chatara	Operation	Lower Barun
Devighat	Operation	Anonymous 12
Trishuli	Operation	Anonymous 12
Marsyangdi	Operation	Thulagi
Middle Marsyangdi	Operation	Thulagi
Upper Marsyangdi A	Operation	Thulagi
Tallo Khare khola	Under construction	Tsho Rolpa
Arun III	Under construction	Lower Barun
Upper Trishuli-1	Under construction	Anonymous 12
Middle Tamor	Under construction	Anonymous 1 & 2
Lower Khare	Generation	Tsho Rolpa
Tamakoshi V	Generation	Tsho Rolpa
Langtang Khola Small	Generation	Anonymous 12
Upper Trishuli 3A	Generation	Anonymous 12
Upper Trishuli 3B	Generation	Anonymous 12
Marsyangdi Besi	Generation	Thulagi
Upper Tamor	Generation	Anonymous 1 & 2
Upper Tamor A	Survey	Anonymous 1
Dudhkoshi 10	Survey	Imja Tsho
Dudhkoshi-9	Survey	Imja Tsho
Rolwaling Khola	Survey	Tsho Rolpa
Lower Isuwa Khola	Survey	Lower Barun
Lower Bom Khola	Survey	Lumding
Luja Khola	Survey	Lumding
Super Inkhu Khola	Survey	Anonymous 11
Upper Inkhu Khola	Survey	Anonymous 11
Bhotekoshi Khola	Survey	Anonymous 12
Lantang Khola Reservoir	Survey	Anonymous 12
Mathillo Langtang	Survey	Anonymous 12
Upper Trishuli-I Cascade	Survey	Anonymous 12
Rigdi Khola	Survey	Thulagi
Dana Khola	Survey	Thulagi
Tamor Mewa	Survey	Anonymous 1 & 2
Tamor Khola-5	Survey	Anonymous 1 & 2 & 3 & 6
Ghunsa-Tamor	Survey	Anonymous 1 & 6
Super Tamor	Survey	Anonymous 1 & 6
Upper Tamor HEP	Survey	Anonymous 1 & 6
Lower Barun Khola	Survey	Lower Barun & Anonymous 9
Upper Barunkhola	Survey	Lower Barun & Anonymous 9
Ghunsa Khola	Survey	Anonymous 2 & 3
Ghunsa Khola	Survey	Anonymous 2 & 3
Chujung Khola	Survey	Anonymous 4 & 5
Dudhkoshi-6	Survey	Imja Tsho, Lumding
Surke Dudhkoshi	Survey	Imja Tsho, Lumding
Hongu Khola I	Survey	Hongu 1& 2, Chamlang, Anonymous 7, 8 & 10
Middle Hongu Khola B	Survey	Hongu 1& 2, Chamlang, Anonymous 7, 8 & 10
Middle Hongukhola A	Survey	Hongu 1& 2, Chamlang, Anonymous 7, 8 & 10
Hongu Khola	Survey	Hongu 1& 2, Chamlang, Anonymous 7, 8 & 10

4.3.3 Damage Assessment

GLOF damage assessment relies on spatial inundation maps of water depth and depth-damage curves. The inundation maps, depicting water depth, are represented by maximum water depths, for areas with flood probabilities greater than 50%. Following the technical manual of the HAZUS Flood model (FEMA, 2009), damage extents of 1% to 10%, 11% to 50%, and 50% to 100% are defined as slight, moderate, and substantial damage, respectively. Table 3 provides estimates of damage to buildings, roads, and agricultural lands for each lake. In the case of Tsho Rolpa Lake, 7,126 buildings are projected to suffer substantial damage from GLOFs. Thulagi Lake and Lower Barun Lake are expected to cause substantial damage to 2,714 and 1,338 buildings, respectively. Other lakes, such as Imja Tsho Lake and Lumding Lake, are estimated to impact roughly 1,000 buildings with substantial damage. Notably, Anonymous 12 (85°37′51″ E, 28°09′44″ N) has the potential to affect 1382 buildings, with 829 experiencing moderate impact and 174 facing substantial damage. Situated in the Trishuli River Basin, Anonymous 12 not only faces a high hazard level (Rank I) but also high exposure. On the other hand, another anonymous lake (Anonymous 13, at 82°40′27″ E, 29°48′09″ N) faces a relatively high hazard level (Rank II) but is not projected to cause any substantial damage to buildings due to GLOFs. For PDGLs with a high number of impacted buildings (more than 1,000), except for Anonymous 12, more than 25% of the impacted buildings are expected to incur substantial damage. In all PDGLs, most affected buildings (over 60%) are predicted to experience moderate or substantial damage. Likewise, over 60% of roads and agricultural lands are anticipated to undergo moderate or substantial damage due to high levels of maximum water depth.

5 Discussion

GLOFs can have a significant impact due to the large volume of water stored in glacial lakes, resulting in rapid breaches, high outflow peaks, and high total discharges. While there is a positive correlation between inundation extent and lake area (Fig 6), it's important to note that inundation propagation and extent also depend on dam breach processes as well as the underlying topography and land surface conditions of downstream areas (Worni et al., 2012; Ancey et al., 2019). Particularly, steep and narrow valley gorges can influence flood waves, causing them to rapidly spread over long distances, often accompanied by significant physical processes such as erosion and the transport of ice, sediment, and debris. Among the 21 PDGLs in Nepal, Tsho Rolpa Lake, Thulagi Lake, and Lower Barun Lake are expected to experience the most severe impacts of GLOFs on buildings and roads, while Tsho Rolpa Lake, Lower Barun Lake, and Lumding Lake are anticipated to be the most impacted in terms of GLOFs on agricultural areas. Rounce et al. (2016, 2017) also assessed the downstream impacts of GLOFs from glacial lakes in the Nepal Himalayas. They likewise identified Tsho Rolpa Lake, Lower Barun Lake, and Thulagi Lake as having the most affected buildings, while two anonymous lakes and Thulagi Lake were anticipated to experience the most significant impacts on agricultural areas. However, it's important to note that Rounce et al. (2016, 2017) employed the Monte Carlo least-cost path model (Watson et al., 2015) to estimate the extent of GLOFs for each lake. While the model is computationally efficient and suitable for large-scale applications, it lacks a physical basis and relies solely on the terrain conditions downstream along the river channel, without considering variations in lake release volumes and peak discharges. As a result, flood extents for lakes with differing potential flood volumes may be indistinguishable. Another limitation is that the threshold for the cut-off distance in MC-LCP needs to be artificially set, while the realistic cutoff distance downstream for each lake varies, sometimes extending over 200 km downstream (Richardson & Reynolds, 2000). This study takes a different approach by employing a physics-based hydrodynamic model that predicts not only the inundation extent but also the spatial characteristics of flood features, including inundation probabilities and water depth while considering various outburst scenarios. This information can be used to identify potential exposures and assess the extent of damage to which exposures may be subject.

In addition to the growing vulnerability of human settlements in mountainous regions, there is an increasing exposure of infrastructure related to energy security and commerce to GLOFs. Therefore, an objective assessment of the risk to

infrastructure posed by PDGLs is crucial. This study considers hydropower plants, given their critical importance and rapid development in Nepal. Nepal is at the heart of a modern resurgence in hydropower development in the Himalayas (Lord et al., 2016). The country boasts abundant hydropower resources thanks to its ample river water, steep gradients, and mountainous terrain. At present, a considerable number of hydropower projects are in the planning and construction stages (46 projects exceeding 100 gigawatts) to enhance the country's overall generating capacity. These planned hydropower projects are primarily situated along rivers connected to glaciers located in the northern region of Nepal (Shakti et al., 2021). While a few existing hydropower plants have experienced direct impacts from recorded GLOFs, such as the Namche hydroelectric power plant destroyed by the 1985 Dig Tsho GLOF (Vuichard & Zimmermann, 1987) and the Bhotekoshi hydropower plant affected by the 2016 GLOF (Cook et al., 2018), GLOFs can be highly destructive and unpredictable, posing a significant threat to hydropower facilities. Furthermore, the expansion of hydropower plants into the upstream regions of watersheds substantially increases the vulnerability of infrastructure to GLOFs (Nie et al., 2021). Schwanghart et al. (2016) estimated that two-thirds of the existing and planned hydropower projects in the Himalayas are located in areas potentially affected by GLOFs, and up to one-third of these projects could face GLOF discharges exceeding their local design flood capacities. In this study, we have identified that 50 existing and planned hydropower projects could potentially be impacted by GLOFs originating from 21 PDGLs. We strongly urge stakeholders responsible for planning, designing, constructing, and managing infrastructure to consider these GLOF risks. It is crucial to develop proactive adaptation measures and adopt sustainable solutions to minimize the negative impacts of GLOFs on infrastructure.

In addition to well-studied PDGLs like Tsho Rolpa Lake, Thulagi Lake, and Lower Barun Lake, some anonymous lakes also present a significant risk of GLOFs. For instance, Anonymous 12, 7, 1, 11, and 2 pose high GLOF risks. Anonymous 12 (85°37′51″ E, 28°09′44″ N), Anonymous 7 (86°55′41″ E, 27°51′00″ N), Anonymous 1 (87°44′59″ E, 27°48′57″ N), and Anonymous 11 (86°51′29″ E, 27°41′13″ N) are categorized as Rank I PDGLs, while Anonymous 2 (87°56′05″ N, 27°47′26″ E; 4950m above sea level) falls into the Rank III category. GLOFs from any of these five lakes have the potential to impact more than 200 buildings, and GLOFs resulting from Lakes Anonymous 12, 1, and 2 may submerge existing hydropower facilities. Unfortunately, there is limited information available about these anonymous lakes in comparison to well-studied PDGLs. To gain a better understanding of their conditions, a comprehensive research strategy is needed, which includes fieldwork investigations, remote sensing techniques, and modeling approaches. This study has leveraged remote sensing techniques and modeling approaches to preliminarily identify PDGLs with a high level of exposure and potential impacts from GLOFs. However, it is imperative to conduct fieldwork investigations, including in situ measurements, to obtain the essential information required to comprehend the actual state of these anonymous lakes at the local scale. These field investigations will also serve as ground truth to calibrate remote sensing-based data and model outputs. Moreover, considering the challenging nature of fieldwork in glacial lake areas, the cost of expeditions, and the high level of fitness and expertise required by monitoring teams, the preliminary identification of PDGLs with high exposure and potential impacts can offer valuable evidence to support decision-making in the allocation of financial and human resources.

We acknowledge the importance of validating the proposed framework for estimating the impact of GLOFs while recognizing the inherent challenges associated with validation due to the limited availability of historical data. Although Nie et al. (2018), Veh et al. (2019), and Shrestha et al. (2023) have provided valuable inventories of historical GLOFs in the Himalayas, these primarily provide information on the date and location of outbursts, offering limited or no information on the actual impacts resulting from historical GLOFs. Even when impact data is available, it often comprises only generalized descriptions, encompassing metrics like the overall number of casualties, infrastructure damage, and affected villages, lacking specific spatial information. Consequently, obtaining adequate data for validating our proposed impact estimation framework for GLOFs proves challenging. It is noteworthy that our proposed framework employs the fully physically based hydrodynamic model HiPIMS, intricately designed to capture the highly transient and complex hydrodynamic processes induced by events

such as dam breaks and flash floods. HiPIMS has been successfully validated for these extreme flow conditions (e.g., Smith and Liang, 2013; Liang et al., 2016). The adoption of this model enhances our confidence in simulating the spatial-temporal processes of GLOF inundation, ultimately contributing to improved hazard evaluation results. Furthermore, we employ Bayesian approaches to derive plausible value ranges for lake volumes and peak discharges. These approaches facilitate the creation of multiple GLOF scenarios for each glacial lake, ensuring comprehensive coverage of all potential glacial lake outburst scenarios. The incorporation of Bayesian methods allows us to account for uncertainties, thereby enhancing the robustness of our impact evaluation for potentially devastating GLOFs.

6 Conclusion

Exposure and damage estimations are integral components of GLOF risk assessment. Having sufficient information about the potential impacts of GLOFs originating from PDGLs is essential to facilitate GLOF risk management. In this study, we harnessed multi-temporal satellite imagery, Bayesian regression models that establish relationships between lake areas and depths, as well as between flood volume and peak discharge, and a high-performance hydrodynamic flood model to support GLOF exposure and damage assessments for multiple lakes. We applied this assessment framework to 21 PDGLs identified in the Nepal Himalaya, and the key findings of this study are summarized as follows:

- Utilizing multi-temporal imagery capturing different hydrological conditions of glacial lakes enables the derivation of the full or maximum glacial lake boundaries for potential risk assessment.

- The Bayesian regression model, which establishes relationships between lake areas and depths, as well as between flood volume and peak discharge, can produce predictive posterior distributions for lake depths and peak discharges for each lake. These distributions offer a plausible range of values for lake volumes and peak discharges for each PDGL, facilitating subsequent objective flood modeling and impact analysis.

- The hydrodynamic model (HiPIMS), supported by parallelized high-performance GPU computation, is capable of predicting the resulting GLOFs in terms of temporally and spatially varying flood frequency and water depths to reflect the highly transient flood dynamics under various scenarios for multiple glacial lakes on a large scale.

- Among the 21 PDGLs identified in the Nepal Himalayas, Tsho Rolpa Lake, Thulagi Lake, and Lower Barun Lake are poised to bear the most severe impacts of GLOFs on buildings and roads. Meanwhile, Tsho Rolpa Lake, Lower Barun Lake, and Lumding Lake will encounter the most significant GLOF impacts on agricultural areas. Four anonymous lakes, specifically Anonymous 12 (85°37′51″ E, 28°09′44″ N), Anonymous 7 (86°55′41″ E, 27°51′00″ N), Anonymous 1 (87°44′59″ E, 27°48′57″ N), Anonymous 11 (86°51′29″ E, 27°41′13″ N), and Anonymous 2 (87°56′05″ N, 27°47′26″ E), have the potential to impact more than 200 buildings. Notably, Anonymous 12, 1, and 2 may even submerge existing hydropower facilities. The GLOFs from these 21 PDGLs can also impact the 12 existing hydropower plants and the 38 hydropower projects that have been granted generation or survey licenses.

Appendix: List of abbreviations used in this study.

CI	confidence interval
DEM	digital elevation model
EVI	Enhanced Vegetation Index
GIS	Geographic Information System
GLOFs	Glacial Lake Outburst Floods

GPU	Graphics processing unit
HDI	highest density interval
HiPIMS	High-Performance Integrated Hydrodynamic Modelling System
MNDWI	Modified Normalized Difference Water Index
NIR	Near Infrared
NDMI	Normalized Difference Moisture Index
NDVI	Normalized Difference Vegetation Index
NDWI	Normalized Difference Water Index
OSM	OpenStreetMap
PDGL	potentially dangerous glacial lake
SRTM	Shuttle Radar Topography Mission
TOA	Top-Of-Atmosphere

References

Ancey, C., Bardou, E., Funk, M., Huss, M., Werder, M. A., & Trewhela, T. (2019). Hydraulic reconstruction of the 1818 Giétro glacial lake outburst flood. *Water Resources Research*, 55(11), 8840-8863.

560   Arcement, G. J., & Schneider, V. R. (1989). Guide for selecting Manning's roughness coefficients for natural channels and flood plains. Washington, DC: US Government Printing Office.

Bajracharya, S. R., Maharjan, S. B., Shrestha, F., Sherpa, T. C., Wagle, N., & Shrestha, A. B. (2020). Inventory of glacial lakes and identification of potentially dangerous glacial lakes in the Koshi, Gandaki, and Karnali River Basins of Nepal, the Tibet Autonomous Region of China. International Centre for Integrated Mountain Development GPO Box, 3226.

565   Barnes, H. H. (1967). Roughness characteristics of natural channels. US Government Printing Office.

Bishop, C. M., & Tipping, M. E. (2003). Bayesian regression and classification. *Nato Science Series sub Series III Computer And Systems Sciences*, *190*, 267-288.

Breiman, L. (2001). Random forests. *Machine learning*, 45(1), 5-32.

Budhathoki, K. P., Bajracharya, O. R., & Pokharel, B. K. (2010). Assessment of Imja Glacier Lake outburst flood (GLOF)

570   risk in Dudh Koshi River Basin using remote sensing techniques. *Journal of Hydrology and Meteorology*, 7(1), 75-91.

Chen, H., Liang, Q., Liang, Z., Liu, Y., & Ren, T. (2020). Extraction of connected river networks from multi-temporal remote sensing imagery using a path tracking technique. *Remote Sensing of Environment*, 246, 111868.

Chen, H., Zhao, J., Liang, Q., Maharjan, S. B., & Joshi, S. P. (2022). Assessing the potential impact of glacial lake outburst floods on individual objects using a high-performance hydrodynamic model and open-source data. *Science of The Total*

575   *Environment*, 806, 151289.

Chow, V.T., (1959). Open-channel Hydraulics. Book Co., New York, McGraw-Hill, p.680.

Cook, K. L., Andermann, C., Gimbert, F., Adhikari, B. R., & Hovius, N. (2018). Glacial lake outburst floods as drivers of fluvial erosion in the Himalaya. *Science*, *362*(6410), 53-57.

Cook, S. J., & Quincey, D. J. (2015). Estimating the volume of Alpine glacial lakes. *Earth Surface Dynamics*, *3*(4), 559-575.

580   Dubey, S., & Goyal, M. K. (2020). Glacial lake outburst flood hazard, downstream impact, and risk over the Indian Himalayas. *Water Resources Research*, *56*(4), e2019WR026533.

Ellison, A. M. (2004). Bayesian inference in ecology. *Ecology letters*, *7*(6), 509-520.

Farr, T. G., Rosen, P. A., Caro, E., Crippen, R., Duren, R., Hensley, S., ... & Alsdorf, D. (2007). The shuttle radar topography mission. *Reviews of geophysics*, 45(2).

585   FEMA. (2009). Multi-hazard loss estimation methodology: Flood model. HAZUS-MH MR3 technical manual. P220.

Gao, B. C. (1996). NDWI—A normalized difference water index for remote sensing of vegetation liquid water from space. *Remote sensing of environment*, *58*(3), 257-266.

Ghimire, M. (2004). Review of studies on glacier lake outburst floods and associated vulnerability in the Himalayas. *Himalayan Review*, 49-64.

590   Granshaw, F. D., & Fountain, A. G. (2006). Glacier change (1958–1998) in the north Cascades national park complex, Washington, USA. *Journal of Glaciology*, *52*(177), 251-256.

Haritashya, U. K., Kargel, J. S., Shugar, D. H., Leonard, G. J., Strattman, K., Watson, C. S., ... & Regmi, D. (2018). Evolution and controls of large glacial lakes in the Nepal Himalaya. *Remote Sensing*, 10(5), 798.

Huete, A., Didan, K., Miura, T., Rodriguez, E. P., Gao, X., & Ferreira, L. G. (2002). Overview of the radiometric and

595   biophysical performance of the MODIS vegetation indices. *Remote sensing of environment*, *83*(1-2), 195-213.

Huggel, C., Kääb, A., Haeberli, W., Teysseire, P., & Paul, F. (2002). Remote sensing based assessment of hazards from glacier lake outbursts: a case study in the Swiss Alps. *Canadian Geotechnical Journal*, *39*(2), 316-330.

Huizinga, J., De Moel, H., & Szewczyk, W. (2017). Global flood depth-damage functions: Methodology and the database with guidelines (No. JRC105688). Joint Research Centre (Seville site).

600   Kapitsa, V., Shahgedanova, M., Machguth, H., Severskiy, I., & Medeu, A. (2017). Assessment of evolution and risks of glacier lake outbursts in the Djungarskiy Alatau, Central Asia, using Landsat imagery and glacier bed topography modelling. *Natural Hazards and Earth System Sciences*, *17*(10), 1837-1856.

Khadka, N., Zhang, G., & Chen, W. (2019). The state of six dangerous glacial lakes in the Nepalese Himalaya. TAO: Terrestrial, *Atmospheric and Oceanic Sciences*, 30(1), 6.

605   Krause, L., Mal, S., Karki, R., & Schickhoff, U. (2019). Recession of Trakarding glacier and expansion of Tsho Rolpa lake in Nepal Himalaya based on satellite data. *Himalayan Geology*, 40(2), 103-114.

Lala, J. M., Rounce, D. R., & McKinney, D. C. (2017). Modeling the glacial lake outburst flood process chain in the Nepal Himalaya: reassessing Imja Tsho's hazard. *Hydrology and Earth System Sciences*, 22, 3721–3737

Lamsal, D., Sawagaki, T., Watanabe, T., & Byers, A. C. (2016). Assessment of glacial lake development and prospects of

610   outburst susceptibility: Chamlang South Glacier, eastern Nepal Himalaya. *Geomatics, Natural Hazards and Risk*, 7(1), 403-423.

Land cover of Nepal 2010 http://rds.icimod.org/Home/DataDetail?metadataId=9224 (2020) Accessed 2020-04-26

Lord, A. (2016). Citizens of a hydropower nation: Territory and agency at the frontiers of hydropower development in Nepal. *Economic Anthropology*, 3(1), 145-160.

615   Liang, Q., Chen, K. C., Jingming, H. O. U., Xiong, Y., Gang, W., & Qiang, J. (2016). Hydrodynamic modelling of flow impact on structures under extreme flow conditions. *Journal of Hydrodynamics*, Ser. B, 28(2), 267-274.

McFeeters, S. K. (1996). The use of the Normalized Difference Water Index (NDWI) in the delineation of open water features. *International journal of remote sensing*, *17*(7), 1425-1432.

Mool, P. K., Maskey, P. R., Koirala, A., Joshi, S. P., Lizong, W., Shrestha, A. B., ... & Shrestha, R. B. (2011). Glacial lakes

620   and glacial lake outburst floods in Nepal. https://policycommons.net/artifacts/1516291/glacial-lakes-and-glacial-lake-outburst-floods-in-nepal/2192662/. Accessed 2022-04-26

Morris, M. W., Hassan, M. A. A. M., & Vaskinn, K. A. (2007). Breach formation: Field test and laboratory experiments. *Journal of Hydraulic Research*, 45(sup1), 9-17.

Muñoz, R., Huggel, C., Frey, H., Cochachin, A., & Haeberli, W. (2020). Glacial lake depth and volume estimation based on

625   a large bathymetric dataset from the Cordillera Blanca, Peru. *Earth surface processes and landforms*, *45*(7), 1510-1527.

Nepal Hydropower portal. (2019) Available at: https://hydro.naxa.com.np/core/about Accessed 22 August 2023.

Nie, Y., Liu, Q., Wang, J., Zhang, Y., Sheng, Y., & Liu, S. (2018). An inventory of historical glacial lake outburst floods in the Himalayas based on remote sensing observations and geomorphological analysis. *Geomorphology*, 308, 91-106.Nie, Y., Pritchard, H. D., Liu, Q., Hennig, T., Wang, W., Wang, X., ... & Chen, X. (2021). Glacial change and hydrological implications in the Himalaya and Karakoram. *Nature reviews earth & environment*, 2(2), 91-106.

Nie, Y., Sheng, Y., Liu, Q., Liu, L., Liu, S., Zhang, Y., & Song, C. (2017). A regional-scale assessment of Himalayan glacial lake changes using satellite observations from 1990 to 2015. *Remote Sensing of Environment*, *189*, 1-13.

OpenStreetMap data for Nepal http://download.geofabrik.de/asia/nepal.html (2015) Accessed 2022-04-26

Rana, B., Shrestha, A. B., Reynolds, J. M., Aryal, R., Pokhrel, A. P., & Budhathoki, K. P. (2000). Hazard assessment of the Tsho Rolpa Glacier Lake and ongoing remediation measures. *Journal of Nepal Geological Society*, 22, 563.

Richardson, S. D., & Reynolds, J. M. (2000). An overview of glacial hazards in the Himalayas. *Quaternary International*, *65*, 31-47.

Rinzin, S., Zhang, G., Sattar, A., Wangchuk, S., Allen, S. K., Dunning, S., & Peng, M. (2023). GLOF hazard, exposure, vulnerability, and risk assessment of potentially dangerous glacial lakes in the Bhutan Himalaya. *Journal of Hydrology*, 619, 129311.

Rodriguez-Galiano, V. F., Ghimire, B., Rogan, J., Chica-Olmo, M., & Rigol-Sanchez, J. P. (2012). An assessment of the effectiveness of a random forest classifier for land-cover classification. *ISPRS journal of photogrammetry and remote sensing*, *67*, 93-104.

Rounce, D. R., McKinney, D. C., Lala, J. M., Byers, A. C., & Watson, C. S. (2016). A new remote hazard and risk assessment framework for glacial lakes in the Nepal Himalaya. Hydrology and Earth System Sciences, 20(9), 3455-3475.

Rounce, D. R., Watson, C. S., & McKinney, D. C. (2017). Identification of hazard and risk for glacial lakes in the Nepal Himalaya using satellite imagery from 2000–2015. *Remote Sensing*, *9*(7), 654.

Sattar, A., Goswami, A., & Kulkarni, A. V. (2019). Hydrodynamic moraine-breach modeling and outburst flood routing-A hazard assessment of the South Lhonak lake, Sikkim. *Science of the total environment*, *668*, 362-378.

Sattar, A., Haritashya, U. K., Kargel, J. S., Leonard, G. J., Shugar, D. H., & Chase, D. V. (2021). Modeling lake outburst and downstream hazard assessment of the Lower Barun Glacial Lake, Nepal Himalaya. *Journal of Hydrology*, *598*, 126208.

Scawthorn, C., Flores, P., Blais, N., Seligson, H., Tate, E., Chang, S., ... & Lawrence, M. (2006). HAZUS-MH flood loss estimation methodology. II. Damage and loss assessment. *Natural Hazards Review*, 7(2), 72-81.

Schaffer-Smith, D., Swenson, J. J., Barbaree, B., & Reiter, M. E. (2017). Three decades of Landsat-derived spring surface water dynamics in an agricultural wetland mosaic; Implications for migratory shorebirds. *Remote Sensing of Environment*, *193*, 180-192.

Schwanghart, W., Worni, R., Huggel, C., Stoffel, M., & Korup, O. (2016). Uncertainty in the Himalayan energy–water nexus: Estimating regional exposure to glacial lake outburst floods. *Environmental Research Letters*, *11*(7), 074005.

Shakti, P. C., Pun, I., Talchabhadel, R., & Kshetri, D. (2021). The Role of Glaciers in Hydropower Production in Nepal. *Journal of Asian Energy Studies*, 5(1), 1-13.

Shrestha, B. B., & Nakagawa, H. (2014). Assessment of potential outburst floods from the Tsho Rolpa glacial lake in Nepal. *Natural Hazards*, *71*(1), 913-936.

Shrestha, F., Steiner, J. F., Shrestha, R., Dhungel, Y., Joshi, S. P., Inglis, S., ... & Zhang, T. (2023). A comprehensive and version-controlled database of glacial lake outburst floods in High Mountain Asia. *Earth System Science Data*, *15*(9), 3941-3961.

Shugar, D. H., Burr, A., Haritashya, U. K., Kargel, J. S., Watson, C. S., Kennedy, M. C., ... & Strattman, K. (2020). Rapid worldwide growth of glacial lakes since 1990. *Nature Climate Change*, *10*(10), 939-945.

Somos-Valenzuela, M. A., McKinney, D. C., Byers, A. C., Rounce, D. R., Portocarrero, C., & Lamsal, D. (2015). Assessing downstream flood impacts due to a potential GLOF from Imja Tsho in Nepal. *Hydrology and Earth System Sciences*, *19*(3), 1401-1412.

Smith, L. S., & Liang, Q. (2013). Towards a generalised GPU/CPU shallow-flow modelling tool. *Computers & Fluids*, 88, 334-343.

Somos-Valenzuela, M. A., McKinney, D. C., Rounce, D. R., & Byers, A. C. (2014). Changes in Imja Tsho in the Mount Everest region of Nepal. *The Cryosphere*, *8*(5), 1661-1671.

Tucker, C. J. (1979). Red and photographic infrared linear combinations for monitoring vegetation. *Remote sensing of Environment*, *8*(2), 127-150.

Tulbure, M. G., Broich, M., Stehman, S. V., & Kommareddy, A. (2016). Surface water extent dynamics from three decades of seasonally continuous Landsat time series at subcontinental scale in a semi-arid region. *Remote Sensing of Environment*, *178*, 142-157.

Veh, G., Korup, O., von Specht, S., Roessner, S., & Walz, A. (2019). Unchanged frequency of moraine-dammed glacial lake outburst floods in the Himalaya. *Nature Climate Change*, 9(5), 379-383.

Veh, G., Korup, O., & Walz, A. (2020). Hazard from Himalayan glacier lake outburst floods. *Proceedings of the National Academy of Sciences*, 117(2), 907-912.

Vuichard, D., & Zimmermann, M. (1987). The 1985 catastrophic drainage of a moraine-dammed lake, Khumbu Himal, Nepal: cause and consequences. *Mountain Research and Development*, 91-110.

Walder, J. S., Iverson, R. M., Godt, J. W., Logan, M., & Solovitz, S. A. (2015). Controls on the breach geometry and flood hydrograph during overtopping of noncohesive earthen dams. *Water Resources Research*, 51(8), 6701-6724.

Walder, J. S., & O'Connor, J. E. (1997). Methods for predicting peak discharge of floods caused by failure of natural and constructed earthen dams. *Water Resources Research*, 33(10), 2337-2348.

Watson, C. S., Carrivick, J., & Quincey, D. (2015). An improved method to represent DEM uncertainty in glacial lake outburst flood propagation using stochastic simulations. *Journal of Hydrology*, *529*, 1373-1389.

Worni, R., Huggel, C., & Stoffel, M. (2013). Glacial lakes in the Indian Himalayas—From an area-wide glacial lake inventory to on-site and modeling based risk assessment of critical glacial lakes. *Science of the Total Environment*, *468*, S71-S84.

Worni, R., Stoffel, M., Huggel, C., Volz, C., Casteller, A., & Luckman, B. (2012). Analysis and dynamic modeling of a moraine failure and glacier lake outburst flood at Ventisquero Negro, Patagonian Andes (Argentina). *Journal of Hydrology*, *444*, 134-145.

Xu, H. (2006). Modification of normalised difference water index (NDWI) to enhance open water features in remotely sensed imagery. *International journal of remote sensing*, *27*(14), 3025-3033.

Yang, M., Cai, Q., Li, Z., & Yang, J. (2023). Uncertainty analysis on flood routing of embankment dam breach due to overtopping failure. *Scientific Reports*, 13(1), 20151.

Yang, Y., Cao, S. Y., Yang, K. J., & Li, W. P. (2015). Experimental study of breach process of landslide dams by overtopping and its initiation mechanisms. *Journal of Hydrodynamics*, 27(6), 872-883.

Yu, X., Hyyppä, J., Vastaranta, M., Holopainen, M., & Viitala, R. (2011). Predicting individual tree attributes from airborne laser point clouds based on the random forests technique. *ISPRS Journal of Photogrammetry and remote sensing*, *66*(1), 28-37.

Zhang, G., Yao, T., Xie, H., Wang, W., & Yang, W. (2015). An inventory of glacial lakes in the Third Pole region and their changes in response to global warming. *Global and Planetary Change*, *131*, 148-157.

Zhao, J., & Liang, Q. (2022). Novel variable reconstruction and friction term discretisation schemes for hydrodynamic modelling of overland flow and surface water flooding. *Advances in Water Resources*, 163, 104187.

Zhang, T., Wang, W., & An, B. (2023a). A conceptual model for glacial lake bathymetric distribution. *The Cryosphere Discussions*, 2023, 1-35.

Zhang, T., Wang, W., An, B., & Wei, L. (2023b). Enhanced glacial lake activity threatens numerous communities and infrastructure in the Third Pole. *Nature Communications*, 14(1), 8250.

715   Zheng, G., Allen, S. K., Bao, A., Ballesteros-Cánovas, J. A., Huss, M., Zhang, G., ... & Stoffel, M. (2021). Increasing risk of glacial lake outburst floods from future Third Pole deglaciation. *Nature Climate Change*, *11*(5), 411-417.

Data availability

The DEM used in this work is the SRTM DEM. Land use types are extracted from the Landsat TM imagery from the year 2010, which can be accessed at http://rds.icimod.org/Home/DataDetail?metadataId=9224.The OpenStreetMap (OSM) data

720   can be accessed via the link http://download.geofabrik.de/asia/nepal.html. Hydropower plant data are obtained from the Hydro Map project through the link https://hydro.naxa.com.np/core/about.

Code availability

The flood model can be accessed through the link https://github.com/HEMLab/HiPIMS-CUDA.

Author contribution

725   HC was responsible for developing the methodology, conducting analysis, and drafting the paper. QL handled funding acquisition, research design, and reviewing and refining the draft. JZ developed the flood model codes, and SM provided a review of the draft.

Competing interests

The contact author has declared that none of the authors has any competing interests.

730   **Acknowledgments**

This work is supported by the WeACT project (NE/S005919/1) funded by the UK Natural Environment Research Council (NERC) through the SHEAR programme.